

Tectonic-climatic coupling drove a mid-pleistocene river piracy in the Northern Qilian Shan, northeastern Tibetan Plateau: Evidence from Isochron $^{26}\text{Al}/^{10}\text{Be}$ Burial Dating and χ analyses[☆]

Qi Su ^{a,*}, Xianyan Wang ^b, Daoyang Yuan ^c, Huiping Zhang ^d, Zhengchen Li ^b, Hao Sun ^c, Hongqiang Li ^c

^a Department of Geography, Faculty of Arts and Sciences, Beijing Normal University, Zhuhai 519087, China

^b School of Geography and Ocean Science, Nanjing University, Nanjing 210023, China

^c School of Earth Sciences, Lanzhou University, Lanzhou 730000, China

^d State Key Laboratory of Earthquake Dynamics and Forecasting, Institute of Geology, China Earthquake Administration, Beijing 100029, China

ARTICLE INFO

Editor: H Falcon-Lang

Keywords:

River piracy
Isochron $^{26}\text{Al}/^{10}\text{Be}$ burial dating
 χ analyses
Earth surface processes
Northeastern Tibetan Plateau

ABSTRACT

River piracy, a dynamic process reshaping drainage networks, plays a pivotal role in landscape evolution, yet its timing and driving mechanisms in active orogens remain poorly constrained. This study focuses on the piracy between the Hongshuiba River and the Zhulongguan River in the northern Qilian Shan (Shan means “mountain” in Chinese), northeastern Tibetan Plateau, to resolve its chronology and geomorphic implications. Utilizing isochron $^{26}\text{Al}/^{10}\text{Be}$ burial dating of fluvial sediments from the abandoned water divide, we determine the piracy occurred at 0.79 ± 0.24 Ma, marking the first radiometric age for such an event in this region. χ analyses reveal pre-piracy disequilibrium in the Zhulongguan River profile, attributed to an earlier piracy by the Beida River, which preconditioned the landscape for subsequent Hongshuiba-Zhulongguan piracy. Integrated results demonstrate that the Hongshuiba-Zhulongguan piracy was driven by tectonic uplift that amplified topographic gradients and the mid-Pleistocene climate transition, which enhanced erosional efficiency. These findings highlight the coupling between northward extension of the Qilian Shan and orbital-scale hydroclimatic variability in triggering threshold-driven drainage reorganization, offering insights into transient landscape responses in active orogens.

1. Introduction

In recent years, more and more researchers are becoming aware that river networks are dynamic features on Earth's surface (Schwanghart and Scherler, 2020; Willett et al., 2014). Tectonic forces and climate fluctuations can alter regional landscapes by disrupting river systems from their equilibrium states. Rivers principally respond to those perturbations by altering their profile slopes (e.g., incision or aggradation) (Kirby and Whipple, 2001), shifting drainage divides (e.g., divide migration) (Bonnet, 2009; He et al., 2024; He et al., 2021), and/or changing the basin topology and geometry (e.g., river piracy) (Bracciali et al., 2015; Fan et al., 2018). Among these, river piracy, which involves diverting the headwaters of one stream into another (Bishop, 1995), can dramatically alter the flow of water and sediment, leading to significant

impacts on water supply (Maher et al., 2007; Yang et al., 2015b), species distribution (Odom and Granger, 2022; Waters et al., 2015), and both long-term and short-term landscape evolution (Fan et al., 2018; Lavé, 2015; Shugar et al., 2017). Previous explorations suggested that piracy in active orogenic belts could further promote the drainage transition from structural-controlled longitudinal rivers to a regional slope-controlled, transverse-dominated drainage network (Babault et al., 2013; Struth et al., 2020).

The Qilian Shan is an actively northwest-southeast trending mountain range that defines the northern boundary of the Tibetan Plateau, nearly 2000 km north of the Himalayan thrust-fold belt (Fig. 1A) (Jolivet et al., 2001; Meyer et al., 1998). Despite its location within the arid Northwest China, the Qilian Shan, recharged primarily by snow/glacier melt and orographic rainfall, serves as a critical water source region

[☆] This article is part of a Special issue entitled: ‘Cenozoic topographic evolution’ published in Palaeogeography, Palaeoclimatology, Palaeoecology.

* Corresponding author.

E-mail address: suqi@bnu.edu.cn (Q. Su).

feeding rivers across surrounding basins (Pan et al., 2010). With the uplift and expansion of the Qilian Shan, those rivers experienced multiple fluvial reorganizations (Meng et al., 2020; Pan et al., 2016; Su et al., 2022), many driven by river piracy (Seong et al., 2011; Su et al., 2022). Based on geomorphic interpretations, previous studies have documented multiple piracy events in northern Qilian Shan (Chu et al., 2015; Seong et al., 2011; Yin and Xu, 1992). A recent study further suggested that all these events were achieved through the capture of longitudinal rivers by transverse rivers (Su et al., 2022). While, the timing and driving mechanisms of these piracy events remains poorly constrained, greatly limiting our understanding on the history and dynamics of regional geomorphic evolution. Among all the piracy events with undefined age, the piracy between the Hongshuiba River and the Beida River has obtained significant attention due to their distinctive topological configurations (Su et al., 2022; Yin and Xu, 1992). The Hongshuiba River and the Beida River have similar topology configurations, as the upper reaches flow along the NWW trending intermontane basins and the lower reaches intersect the subparallel ranges (Fig. 1B). The Zhulongguan River, one of tributaries of the Beida River, shares a common intermountain valley with the upper reach of the Hongshuiba River, and the divide between the two reaches is wide and low (Fig. 2A). Previous studies distinguished the piracy features, including the pirated stream, beheaded channel, wind gap and the elbow of capture (Su et al., 2022; Yin and Xu, 1992).

In recent years, isochron $^{26}\text{Al}/^{10}\text{Be}$ burial dating has been widely used to date landscape evolution (Bender et al., 2016; Erlanger et al., 2012; Granger et al., 2022). The development of the isochron burial dating method, which determines ages by statistically analyzing multiple samples from a single burial horizon while excluding reworked clasts through isotopic screening (Granger et al., 2015; Odom and Granger, 2022), has significantly expanded the range of suitable sites and improved dating reliability. In this study, we directly dated the abandoned fluvial deposits on the wide, low-relief water divide between the Hongshuiba River and Zhulongguan River, and interpreted the resulting age as the timing of the piracy event. Subsequently, the geomorphic analyses (e.g., bedrock river profile analyses (Perron and Royden, 2013)) were conducted for the two drainage basins to reconstruct the landscape characteristics prior to piracy. Finally, we discuss the implications of these findings for the geomorphic evolution of the northern

Qilian Shan.

2. Background setting

The original configuration of the Qilian Shan was established before the Cenozoic, due to the closure of the Qilian Ocean during the Ordovician-Silurian (Yin et al., 2008; Zuza et al., 2017). After that, the proto-Qilian Shan experienced the Jurassic-Cretaceous extension and subsequent early Cretaceous contractional deformation, which led to regionally extensive thrusting and folding (Jolivet et al., 2001; Zuza et al., 2018). As the consequence of the India-Asia collision and subsequent continuous convergence, the Qilian Shan underwent extensive intracontinental deformation during the Cenozoic, and involved mixed thrusting and strike-slip faulting, leading to widespread crustal shortening (Fig. 1B) (Allen et al., 2017; Meyer et al., 1996). In addition, the active crustal shortening is geomorphologically accommodated by the exhumation and uplift of the subparallel NW-SE striking ranges (Lease et al., 2011; Yu et al., 2019; Zheng et al., 2017). In the central-northern Qilian Shan, studies on low-temperature thermochronology and provenance analyses imply a gradual northward activation of successive subranges from the Miocene to the Pliocene (Pang et al., 2019; Zheng et al., 2017). The successive NW-SE striking ranges are separated from adjacent intermontane valleys (i.e., sub-basins) and piedmont basins by thrust faults, and supply detrital materials for its southern and northern sedimentary basins and small basins located therein (Dai et al., 2005; Fang et al., 2003; He et al., 2020). The Qilian Shan, including the NW-SE striking subranges, exhibits a zonation of sedimentary and metasedimentary rocks, trending WNW-ESE, in the Ordovician-Silurian ages. Rock types encountered include sedimentary clastic rock assemblages, low-grade metamorphic rocks, mafic igneous rocks, ocean carbonates, and silicates (Rong et al., 2019; Zhang et al., 2019). In addition, plagioclase granite intrusions from the Caledonian orogeny are also present in the northern Qilian Shan (Cheng et al., 2019).

Located within the arid region of Northwestern China, the Qilian Shan still experiences an annual precipitation ranging between 50 and 600 mm. Precipitation distribution is strongly influenced by the topography, with the highest rainfall occurring near the crest of the range and decreasing towards the Piedmont plains (Hu et al., 2010; Pan et al., 2010). In addition, the regional rainfall also expresses a decreasing trend

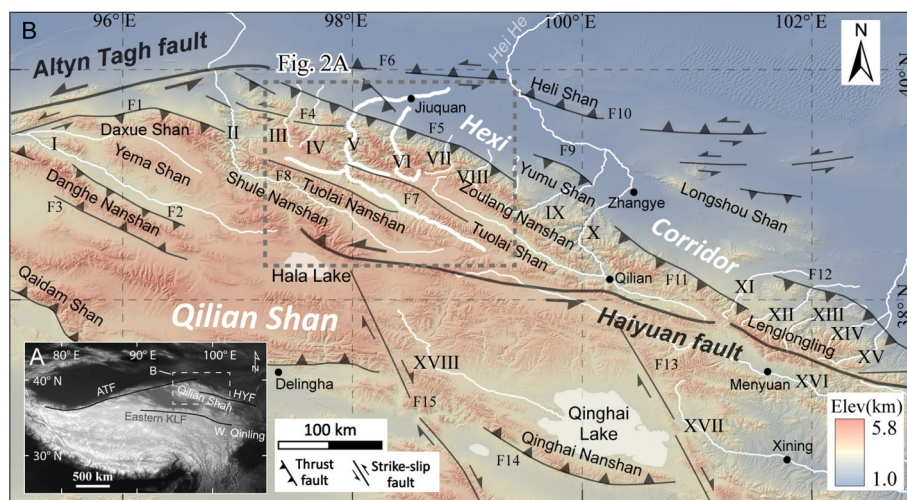


Fig. 1. (A) Tectonic and geomorphic units of the Tibetan Plateau. AFT- Altyn Tagh Fault; HYF-Haiyuan Fault; KLF-Kunlun Fault. (B) Geomorphic characteristics and major faults of the Qilian Shan. The locations of active faults are adopted from (Yuan et al., 2013). The bold white lines show the target rivers analyzed in this study. I-Danghe River, II-Shule River, III-Shiyou River, IV-Baiyang River, V-Beida River, VI-Hongshuiba River, VII-Fengle river, VIII-Maying River, IX-Liyuan River, X-Heihe River, XI-Xida River, XII-Dongda river, XIII-Jinta River, XIV-Zamu River, XV-Huangyang River, XVI-Datong River, XVII-Huangshui River, XVIII-Buha River. F1-Daxueshan Fault, F2-North Danghe Nanshan Fault, F3-South Danghe Nanshan Fault, F4-Changma Fault, F5-Fodongmiao-Haongyazi Fault, F6-Jinta Nanshan Fault, F7-Tuolai Nanshan Fault, F8-Tuolai Nanshan Fault, F9-Yumushan Fault, F10-Helishan Fault, F11Minle-Damaying Fault, F12-South Wuwei Fault, F13-Riyueshan Fault, F14-Qinghai Nanshan Fault, F15-Elashan Fault.

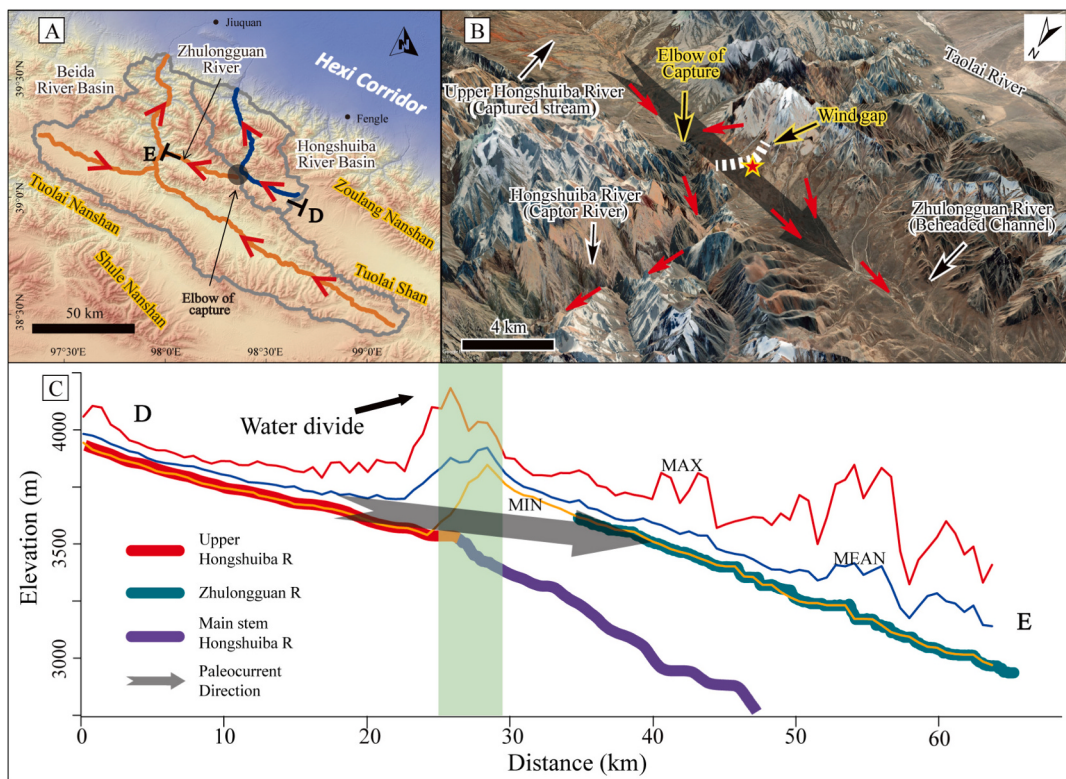


Fig. 2. (A) Geomorphic characteristic of Beida River and Hongshuiba River. The orange line represents the Beida River and the blue line shows the location of the Hongshuiba River. The red arrows show the current directions of the river flow. (B) The geomorphic environment of the captor river and pirated River. The base map is adopted from Google Earth. The white dotted line shows the location of the water divide, and the red star shows the location of our sampling point. The grey arrow indicates the direction of the river flow before the river piracy. (C) River profiles of the Hongshuiba River and Zhulongguan River. In addition, the grey arrow shows the direction of the river flow before the piracy. In addition, the red, blue and orange lines in the figure represent the highest, average and lowest values in the terrain profile respectively, distinct from the river profiles. The location of the swath profile can be found in Fig. 2A. Fig. 2C is modified from Su et al. (2022). (For interpretation of the references to colour in this figure legend, the reader is referred to the web version of this article.)

from east to west, implying that the moisture may be transported by the East Asian Monsoon. Large rivers originating from the northern Qilian Shan, including the Danghe River, the Shule River, the Heihe River, and the Shiyang River (Fig. 1B), are jointly recharged by regional precipitation and mountain glaciers. Located on the western portion of the northern Qilian Shan, the Beida River, and the Hongshuiba River have attracted attention because of their characteristic topology configurations (Fig. 2A). Previous results on longitudinal profiles of the two rivers suggested that the upstream of the Hongshuiba River may have flowed into the Zhulongguan River, implying that the two reaches can be reconstructed as a large, single paleo-Zhulongguan River (Su et al., 2022) (Fig. 2).

3. Methods

3.1. ^{26}Al - ^{10}Be Isochron Burial Dating

Given that the previous results, derived from numerical simulation and geomorphic deduction, suggested that the river piracy may have occurred no earlier than the early Pleistocene (Su et al., 2022; Yin and Xu, 1992), we expected that the true age of the piracy event may fall within the age range that the isochron burial method works well (i.e., ~0.3–5.0 Ma).

In this study, we utilize the isochron ^{26}Al - ^{10}Be burial dating method to estimate the abandonment age for the wide and low gravels-capping water divide, and establish constraints on the timing of river piracy. The isochron method was first used to determine the burial age of materials experiencing complex exposure-burial history (Balco and Rovey, 2008). It has since been widely used and successfully applied to date glacial

events (Akçar et al., 2017), fluvial incision and terrace abandonment (Litty et al., 2018; Odom and Granger, 2022; Zhao et al., 2016), and the occupation and dispersal of early hominins (Granger et al., 2015; Tu et al., 2022).

The isochron method is generally based on the principle that the clasts from a single stratigraphic horizon (buried by several meters of sediment sufficient to minimize post-burial production) should span a range of pre-burial isotope concentrations, but have identical post-burial production, no matter how complicated the burial history is (Erlanger et al., 2012). Therefore, the post-burial component is usually treated as a constant among samples:

$$N_{26} = N_{26,\text{inh}} e^{-t/\tau_{26}} + C_{26} \quad (1)$$

$$N_{10} = N_{10,\text{inh}} e^{-t/\tau_{10}} + C_{10} \quad (2)$$

where N is the measured nuclide concentration, N_{inh} represents the decayed inherited component, and C expresses the post-burial constant component, with the subscripts 26 and 10 referring to ^{26}Al and ^{10}Be . Eqs. 1 and 2 are usually used to solve for $N_{26,\text{inh}}/N_{10,\text{inh}}$ which is usually expressed as the ratio of inherited nuclide concentrations R_{inh} :

$$(N_{26} - C_{26}) / (N_{10} - C_{10}) = \left(\frac{N_{26,\text{inh}}}{N_{10,\text{inh}}} \right)^{e^{-t/\tau_{\text{bur}}}} = R_{\text{inh}} e^{-t/\tau_{\text{bur}}} \quad (3)$$

where τ_{bur} (the subscript “bur” means burial) is the effective mean life for the $^{26}\text{Al}/^{10}\text{Be}$ ratio which is given by the following equation:

$$\tau_{bur} = \frac{1}{\frac{1}{\tau_{26}} - \frac{1}{\tau_{10}}} \quad (4)$$

The mean life of ^{26}Al is taken as 1.021 ± 0.024 Ma and that of the ^{10}Be is adopted as 2.005 ± 0.017 Ma (Chmeleff et al., 2010; Nishiizumi, 2004), leading to an effective burial mean life $\tau_{bur} = 2.08 \pm 0.1$ Ma. At this time, we can solve for N_{26} in terms of N_{10} , as shown in:

$$N_{26} = N_{10} R_{inh} e^{-t/\tau_{bur}} - C_{10} R_{inh} e^{-t/\tau_{bur}} + C_{26} \quad (5)$$

Several studies have demonstrated that the R_{inh} may change with latitude and/or altitude (Borchers et al., 2016; Corbett et al., 2017). In this study, we used the constant R_{inh} value of 6.8, which has been widely employed in East Asia, including the west Kunlun Mountains (Zhao et al., 2016), the southeastern Tibetan Plateau (Liu et al., 2022), the southern and northwestern China (Luo et al., 2020; Tu et al., 2017).

During the field investigation, we found that the capping gravels, which originated from the northern Qilian Shan, contain quartz-bearing clasts, allowing measurement of in situ cosmogenic-nuclide concentrations to determine the burial age. Therefore, we collected samples from at least 4.5 m below the top of the gravel-capping water divide. All the samples were constrained within a 10–15 cm thick horizon (Fig. 3). The collected samples, including quartz-bearing cobbles, mixed pebbles, and amalgamated sand, were analyzed for quartz, as different sizes in targeted samples could ensure that the samples experienced various pre-burial histories, which are favorable for isochron analysis.

All sample processing, including the physical and chemical quartz isolation and purification, sample dissolution, carriers (i.e., ^9Be -carrier) addition, anion-exchange and cation-exchange chromatography, and transformation into oxides were performed at the State Key Laboratory of Cryospheric Science and Frozen Soil Engineering, Northwest Institute of Eco-Environment and Resources, Chinese Academy of Sciences (CAS), following the standard lab protocols (Su et al., 2023; Zhao et al., 2023). The cosmogenic concentration measurements were conducted at the Xi'an Accelerator Mass Spectrometer (AMS) center, State Key Laboratory of Loess Science, Institute of Earth Environment, CAS. The measured $^{10}\text{Be}/^{9}\text{Be}$ ratios were normalized to the ICN AMS standard ($^{10}\text{Be}/^{9}\text{Be} = 2.851 \times 10^{-12}$, 07KNSTD), and the $^{26}\text{Al}/^{27}\text{Al}$ ratios were normalized to the ICN AMS standard ($^{26}\text{Al}/^{27}\text{Al} = 1.065 \times 10^{-11}$, KNSTD) (Zhou et al., 2020).

3.2. χ analyses

Bedrock erosion exhibits scaling behavior that can be described by either the unit stream power or shear stress. Both of these relationships contribute to the development of a model for river incision into bedrock, specifically in cases of detachment-limited behavior (Howard et al., 1994; Whipple, 2004). One of the most widely used models (the stream power incision model) suggests that the bedrock incision rate can be expressed by the channel slope (S) and river discharge (Q), although the latter one is always replaced by the drainage area (A) (Kirby and Whipple, 2012; Wobus et al., 2006). When considering the tectonic-derived rock uplift rate (U), one can model the elevation (z) of any point on the bedrock channel, with the elevation changing with time (t). In our study, the model is presented as:

$$\frac{\partial z(t, x)}{\partial t} = U(t, x) - E(t, x) = U(t, x) - KA^m \left[\frac{\partial z(t, x)}{\partial x} \right]^n \quad (6)$$

where K represents a constant that relates to the regional physical environments, including bedrock erodibility and climate, and m and n are empirical constants corresponding to drainage area and channel slope, respectively (Kirby and Whipple, 2012).

If assuming that U and K are uniform throughout the drainage and time-invariant, we can integrate eq. 6 using a coordinate transformation (Perron and Royden, 2013). This yields a linear elevation profile expressed through the integral quantity, χ :

$$z(x) = z(x_b) + \left(\frac{U}{KA_0^m} \right)^{\frac{1}{n}} \chi \quad (7)$$

where χ is defined by integration in the upstream direction from base level x_b to observation point x :

$$\chi = \int_{x_b}^x \left(\frac{A_0}{A(x)} \right)^{\frac{m}{n}} dx \quad (8)$$

Here, A_0 is an arbitrary scaling area typically set to 1 for unit consistency, and the resulting Eq. 7 describes a straight line (the χ profile) with elevation z on the vertical axis and the integral quantity χ on the horizontal axis. Physically, this transformation quantifies the cumulative effect of drainage area variations along the channel network, where larger χ values correspond to positions with smaller upstream drainage areas under steady-state conditions (Willett et al., 2014).

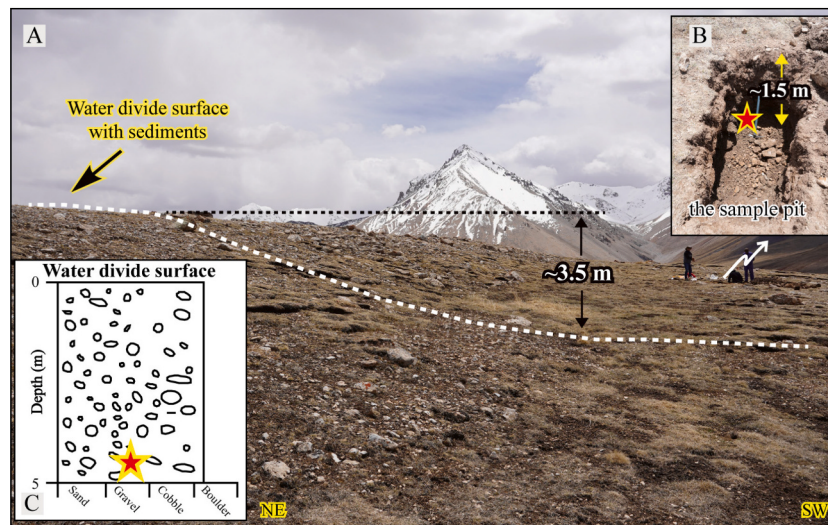


Fig. 3. (A) Capping gravels on the water divide; (B) The sampling pit excavated 3.5 m below the top of the water divide; (C) The stratigraphic section of the sampling pit on the water divide. The red stars show the sampling point. It can be noted that our samples are capped by ~4.7 m thick fluvial sediments when targeted. (For interpretation of the references to colour in this figure legend, the reader is referred to the web version of this article.)

χ -profiles for both drainages before (i.e., the paleo-Zhulongguan River and the paleo-Hongshuiba River) and after the piracy (i.e., modern profiles) were reconstructed. For the paleo-Hongshuiba River, the drainage area downstream of the “Elbow of Capture” in the modern Hongshuiba River was used in the reconstruction. For the paleo-Zhulongguan River, the river profile was extended to the water divide along the shortest linear path. The drainage area upstream of the “Elbow of Capture” in the modern Hongshuiba River was also included in the reconstruction. The detailed theoretical derivation and operation process used in this study can be found in (Fan et al., 2018). In this study, the χ profiles of the Hongshuiba River and the Zhulongguan River were conducted based on the NASADEM, using ChiProfiler (Gallen and Wegmann, 2017) and TopoToolbox (Schwanghart and Scherler, 2014). These profiles were constructed assuming uniform regional U and K, with a concavity value of 0.43 adopted from (Wang et al., 2019).

4. Results

4.1. ^{26}Al — ^{10}Be Isochron Burial Dating

The ^{26}Al and ^{10}Be concentrations of the samples were determined (Table. 1). In the calculation of nuclide concentrations, we have subtracted blank values measured during AMS analysis. The $^{10}\text{Be}/^{9}\text{Be}$ ratio of the blank was 1.16E-15 with a 100 % uncertainty, and the $^{26}\text{Al}/^{27}\text{Al}$ ratio of the blank was 1.81E-15, also with 100 % uncertainty. In order to successfully apply the isochron burial method, ^{26}Al and ^{10}Be concentrations of samples before burial should vary widely, and our results satisfy this essential requirement. The highest concentrations come from the sample FSL-1, with concentrations of $43,300 \pm 2000$ atoms/g for ^{10}Be and $227,000 \pm 19,600$ atoms/g for ^{26}Al . The lowest concentrations come from the sample FSL-2 ($11,700 \pm 720$ and $98,400 \pm 7200$ atoms/g), indicating quite low ^{26}Al — ^{10}Be concentrations before burial.

Table 1. Cosmogenic nuclide concentrations of samples from the water divide.

After acquiring the cosmogenic concentrations, the isochron burial age was determined by the Python-based Pysochron (Odom, 2025). The software applies orthogonal distance regression in tandem with Monte Carlo resampling: each measurement is perturbed by Gaussian noise and refit 1000 times to generate synthetic burial isochrons. Simulations yielding non-physical results, for example, the negative ages, ages exceeding ten half-lives of ^{10}Be , negative post-burial production rates, or slope values far outside the surface production ratio, are excluded. The remaining ensemble of intercepts and slopes is then used to derive the mean burial age and its 1σ uncertainty, alongside MSWD and automated outlier flags. For the water-divide gravel deposits, Pysochron’s continuous-erosion model and default production ratios were retained, and 1000 orthogonal-regression Monte Carlo iterations were performed to establish final burial ages with 2σ uncertainties. Our data is presented in Fig. 4, with the best-fitting isochron age of 0.79 ± 0.24 Ma.

4.2. χ analysis

Before the piracy, the χ -profile of the paleo-Zhulongguan River shows a distinct knickpoint, or a knickzone, with a steep lower reach and a flattened upper reach. While the χ -profile of the paleo- Hongshuiba River exhibits a nearly equilibrium state and shares a similar trend with the lower part of the paleo- Zhulongguan River (Fig. 5 A). After the river piracy, the Hongshuiba River obtained a substantial drainage area at the cost of the Zhulongguan River. This piracy made the profile of the paleo-Hongshuiba River move towards lower χ values and become steeper, compared with those before piracy (Fig. 5B). The captured reach (i.e., the modern upper Hongshuiba River), seems to maintain its original slope, forming a distinct inflection zone in the chi plot. Correspondingly, the Zhulongguan River has moved towards higher χ values, as it is directly influenced by the removal of the upstream drainage area.

Table 1
Cosmogenic nuclide concentrations of samples from the Fenshui Liang site.

Sample No.	Sample weight (g)	Sample type	$^{10}\text{Be}/^{9}\text{Be}$ ratio		Carrier Weight (g)	^{10}Be concentration (atoms/g)	^{10}Be Error value (atoms/g)	$^{26}\text{Al}/^{27}\text{Al}$ ratio	$^{26}\text{Al}/^{27}\text{Al}$ Uncertainty (%)	Total Al concentration (atoms/g)	^{26}Al Total Al value (atoms/g)	^{26}Al Error value (atoms/g)	$^{26}\text{Al}/^{10}\text{Be}$ ratio
			Uncertainty (%)	(%)									
FSL-1	25.3	sand	6.26E-14	4	0.262	43,200	2000	6.63E-14	8.36	3,952	227,000	19,600	5.28 ± 0.51
FSL-2	36.5	sandstone	2.53E-14	3.7	0.261	11,700	720	5.17E-14	6.65	3,202	98,400	7200	8.48 ± 0.80
FSL-3	33.8	metasandstone	5.95E-14	5.46	0.262	30,700	1800	7.94E-14	6.74	3,680	190,000	13,300	6.24 ± 0.57
FSL-4	31.27	metasandstone	7.25E-14	4.91	0.262	40,600	2100	1.04E-13	7.76	3,465	254,000	20,200	6.30 ± 0.59
FSL-5	38.06	conglomerate	4.06E-14	3.6	0.259	18,200	1000	6.81E-14	6.99	3,770	148,000	10,800	8.19 ± 0.74

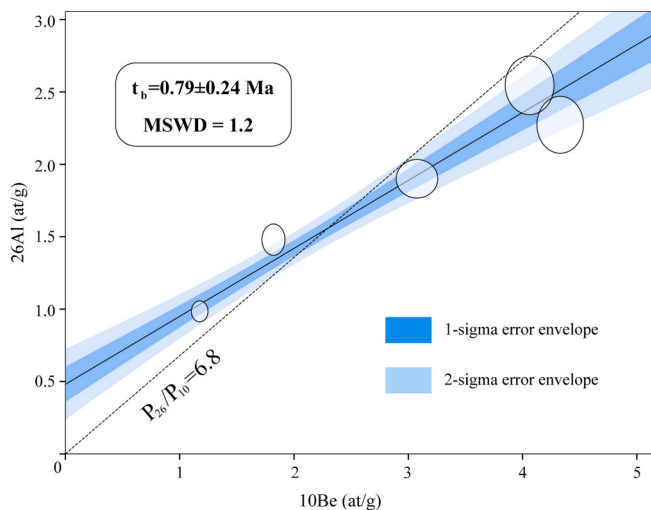


Fig. 4. Isochron burial dating result for the samples taken from the Zhulongguan-Hongshuiba water divide. Each cross represents an individual sample, showing 1-sigma error ellipses. The best-fit isochron with 1-sigma uncertainty indicates an age of 0.79 ± 0.24 Ma.

5. Discussion

In this study, burial dating using the isochron method with $^{26}\text{Al}/^{10}\text{Be}$ on 5 samples collected from the water divide yields an age of 0.79 ± 0.24 Ma (Fig. 6). This chronological result marks the first radiometric age determined for river piracy in the northern Qilian Shan, filling a critical gap in understanding the spatiotemporal progression of drainage reorganization along the northeastern Tibetan Plateau. Our finding aligns reasonably well with the result from previous geomorphic deduction (i.e., no earlier than the early Pleistocene) (Yin and Xu, 1992), while predating the outcome of prior numerical simulations (i.e., ~ 0.35 Ma) (Su et al., 2022).

5.1. Discrepancy with previous results

The marked disparity between our cosmogenic isochron burial age (i.e., 0.79 ± 0.24 Ma) and the ~ 0.35 Ma piracy timing inferred from numerical modeling (Su et al., 2022), likely arises from inherent limitations in simulating complex geomorphic thresholds. Numerical simulations reconstruct piracy timing through inverted fluvial incision histories, but inherently depend on simplifications such as uniform lithology, time-invariant uplift rates, and equilibrium sediment flux (Fox, 2019; Wang et al., 2022b). Such idealized assumptions, however, are seldom fully satisfied in natural systems, and their inherent limitations

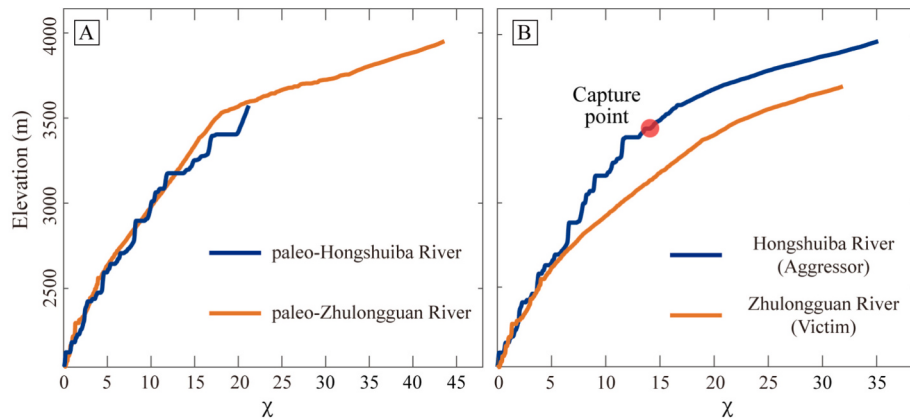


Fig. 5. (A) χ plots for the paleo-Hongshuiba River and paleo-Zhulongguan River before capture. (B) χ plots for the present Hongshuiba River and Zhulongguan River.

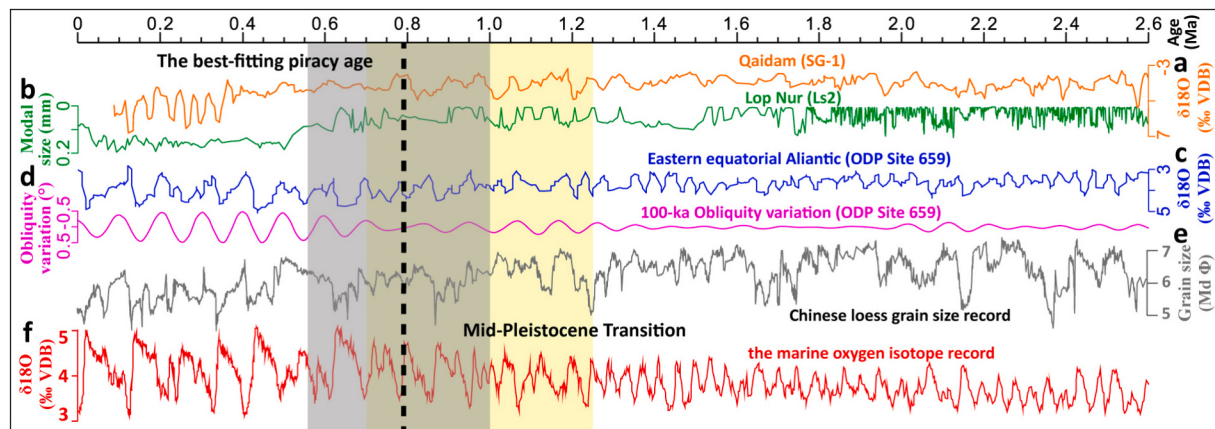


Fig. 6. Records of climate change since 2.6 Ma. The yellow shaded area denotes the mid-Pleistocene climate transition, and the black dotted line and grey shaded area indicate the timing of fluvial piracy, respectively. (a) Carbonate $\delta^{18}\text{O}$ records from Drill SG-1, Qaidam basin (Han et al., 2020). (b) Modal grain-size records from Drill Ls2, Lop Nur (Liu et al., 2020). (c&d) Benthic $\delta^{18}\text{O}$ records and obliquity variation from ODP site 659 (Zachos et al., 2001). (f) High-resolution grain size records from five loess sections, located at Baoji, Lingtai, Jingchuan, Puxian, and Pingliang in the southern and middle Loess Plateau (Ding et al., 2002). (e) The benthic $\delta^{18}\text{O}$ records since 5.3 Ma (Lisiecki and Raymo, 2005). (For interpretation of the references to colour in this figure legend, the reader is referred to the web version of this article.)

prevent robust representation of temporally staggered geomorphic responses associated with multi-stage landscape evolution. For example, critical uncertainties in model parameterization that depend on regional climatic condition and lithology (e.g., erosion coefficient K and concavity exponent m/n) could strongly amplify output variability (Wang et al., 2022a; Zhang et al., 2023) and overestimated erosional efficiency would artificially shorten the timescale required to achieve observed channel profiles. In addition, modeled ages may reflect post-piracy knickpoint propagation rather than the initial capture event, as erosional responses to discharge transfer often lag behind divide destabilization (Bian et al., 2024; Ye et al., 2024).

In contrast, our isochron burial age (i.e., 0.79 ± 0.24 Ma) directly dates the sequestration of pre-piracy sediments, providing a near-instantaneous record of paleo-channel abandonment. The robustness of this method is underscored by its insensitivity to post-capture erosion dynamics (Bender et al., 2020; Odom and Granger, 2022), which instead challenge numerical simulations. We thus posit that the ~ 0.79 Ma age better approximates the true timing of piracy, whereas the younger modeled age likely captures subsequent landscape adjustments rather than the capture event itself. This highlights the critical need to ground-truth numerical frameworks with direct chronometric constraints when resolving transient geomorphic event.

5.2. The Piracy before the Hongshuiba-Zhulongguan piracy

The subdued upper paleo-Zhulongguan River morphology, characterized by anomalously low channel steepness (k_{sn}) and χ -profile flattening, contrasts sharply with the state of its lower reach (Fig. 5 A), indicating that the paleo-Zhulongguan River was in a state of disequilibrium (Willett et al., 2014), and similar to the modern Hongshuiba River (Fig. 5B). A recent study suggested that glacial erosion can decrease mountain peaks and create gentle valley floors with low stream power in highly glaciated regions (Lai and Huppert, 2023; Lai and Huppert, 2024). While Quaternary glaciations sculpted high-elevation landscapes in the Qilian Shan (Equilibrium Line Altitude: 4500–4600 m) (Hu et al., 2014), the Zhulongguan River's elevation (3000–3800 m) lies far below the glacial influence zone, ruling out ice-marginal processes as the driver of this disequilibrium.

Instead, the χ -anomaly of the paleo-Zhulongguan River aligns well with geomorphic signatures of river piracy (Han et al., 2024; Willett et al., 2014). After a river capture event, the newly integrated river segments usually exhibit distinct disequilibrium features in χ -plots due to abrupt drainage area redistribution (Bian et al., 2025; Willett et al., 2014; Yang et al., 2015a). The captor river gains increased drainage area (A) at the capture point, which enhances its erosive power ($K \cdot A^m \cdot S^n$) and lowers its steady-state elevation profile. This forces the χ -plot segment below the capture point to steepen sharply as the channel rapidly incises to equilibrate with the new area-augmented erosion dynamics (Whipple et al., 2017b; Willett et al., 2014). Meanwhile, the captured reach retains its pre-capture χ -profile, which becomes anomalously gentle relative to the captor's adjusted downstream profile, creating a sharp χ -slope discontinuity that reflects the transient imbalance between inherited topography and post-capture erosional dynamics (Whipple et al., 2017a). We attribute this disequilibrium of the paleo-Zhulongguan River to an initial piracy event which clearly predates the Zhulongguan-Hongshuiba piracy, when the paleo-Beida River, a transverse antecedent stream, captured the axial Zhulongguan valley (Fig. 2A). This piracy redistributed discharge, abruptly lowering the base level of the Zhulongguan's upper reach and inducing a wave of regressive incision that propagated headward at rates modulated by bedrock erodibility, imprinting a legacy of χ profile flattening that persisted until the mid-Pleistocene piracy between the Hongshuiba River and Zhulongguan River.

5.3. Tectonic-climatic forcing piracy in the northern Qilian Shan

The sequential piracy events between the Beida River, Hongshuiba River, and Zhulongguan River within a short geological timeframe may highlight a dynamic interplay between tectonic uplift and climatic oscillations. The northward propagation of the Qilian Shan since the Miocene has generated NWW-SEE trending ranges separated by longitudinal valleys (Meyer et al., 1998; Zheng et al., 2017; Zheng et al., 2013) (Fig. 1B). These valleys, initially occupied by structurally controlled longitudinal rivers (e.g., paleo-Zhulongguan River) (Meng et al., 2020), became prone to capture as ongoing uplift amplified regional topographic gradients (Hu et al., 2021; Su et al., 2022). In addition, the Paleozoic sedimentary-metamorphic rocks along the Zhulongguan-Hongshuiba divide developed pervasive joint systems (Wang et al., 2014), creating mechanically weak zones susceptible to fluvial erosion. Consequently, river piracy in the northern Qilian Shan occurred as slope-controlled transverse rivers intersected the mountain ranges and captured the longitudinal rivers in the axial mountain valleys. Critically, the initial Beida-Zhulongguan piracy destabilized the regional drainage network (Su et al., 2022), leaving the pirated Zhulongguan River in a transient state with a flattened upper χ -profile (Fig. 5 A). This disequilibrium preconditioned the landscape for the subsequent Zhulongguan-Hongshuiba piracy at 0.79 ± 0.24 Ma, as headward erosion along the paleo-Hongshuiba River exploited both inherited structural weaknesses and sediment flux imbalances (Fan et al., 2018; Willett et al., 2014) triggered by the earlier piracy.

The mid-Pleistocene Hongshuiba-Zhulongguan piracy also coincides with the intensified East Asian monsoon variability during the Mid-Pleistocene Transition (MPT; ~ 1.2 – 0.7 Ma) (Fig. 6). Enhanced seasonal precipitation increased peak discharges in transverse drainages like the paleo-Hongshuiba River (Berends et al., 2021; Herbert, 2023), enabling divide breaching through two coupling mechanisms: (1) elevated shear stress during extreme runoff events (Claude et al., 2019; Mauffrey et al., 2017) accelerated incision into pre-fractured sedimentary-metamorphic rocks, while (2) interglacial warming (e.g., Marine Isotope Stage 17, (Sánchez Goñi et al., 2019)) reduced permafrost cementation along bedrock fractures, promoting hillslope destabilization.

In essence, the Hongshuiba-Zhulongguan piracy, occurred during the middle Pleistocene (i.e., 0.79 ± 0.24 Ma), represents an additional event following the earlier Beida-Zhulongguan piracy. It falls within the context of a climate-tectonic coupling with continuous uplift and outward expansion of the northern Qilian Shan (Cheng et al., 2019; Liu et al., 2010; Zheng et al., 2017) and dramatic climate fluctuations since the late Cenozoic (Han et al., 2020; Lisiecki and Raymo, 2005; Zachos et al., 2001). Sustained uplift of the northern Qilian Shan (1.0 ± 0.5 mm/a since the mid-Miocene) (Hetzell et al., 2019; Yang et al., 2018; Zheng et al., 2010) provides a tectonic foundation for this climate-tectonic coupling. Such uplift rates maintained critical topographic gradients, amplifying erosional efficiency during high-discharge episodes driven by orbital-scale hydroclimatic forcing (Gnann et al., 2025; Willett, 2025). The climate-tectonic coupling is also evidenced by χ -profiles after the Hongshuiba-Zhulongguan piracy (Fig. 5B), where steepened knickzone slopes reflect both sustained uplift of the northern Qilian Shan and pulsed fluvial erosion during high-discharge intervals. In this study, the ~ 0.79 Ma age also captures a threshold response to orbital-scale hydroclimatic forcing superimposed on the region's northward extension deformation field, a paradigm where climate oscillations amplify tectonically preconditioned drainage instability.

5.4. Geomorphic significance

The mid-Pleistocene Hongshuiba-Zhulongguan piracy event exemplifies a broader paradigm of drainage reorganization in active orogens, where tectonic propagation primes landscapes for threshold-driven captures amplified by climatic forcing. Globally, river piracy has been

implicated in the rapid deformation of orogenic plateaus (e.g., river capture in the eastern Himalaya, (Bracciali et al., 2015; Jaiswara et al., 2019) and drainage reorganization in the eastern Cordillera plateau, (Struth et al., 2020; Struth et al., 2017)) and the abrupt redirection of sediment fluxes that modulate orogen and foreland basin dynamics (e.g., Forty-mile-Ysynukon piracy in the eastern Alaska, (Bender et al., 2020) and Dadu-Anning piracy in the eastern Tibetan Plateau, (Yang et al., 2020; Zheng et al., 2023)). The Qilian Shan case study uniquely bridges these endmember scenarios: like the Himalaya, its piracy events reflect northward crustal shortening and divide migration, yet similar to the eastern Alaska, the cascading effects of piracy (e.g., knickzone propagation, sediment pulse generation) are demonstrably modulated by orbital-scale climate oscillations. This duality underscores river piracy as a universal mechanism for transient landscape rejuvenation in active orogens (Babault et al., 2013; Penserini et al., 2024; Struth et al., 2020; Su et al., 2022), capable of overriding steady-state erosion patterns dictated by tectonic uplift alone. Critically, the ~0.79 Ma age, anchored by direct isochron burial dating, provides a rare chronometric benchmark for testing numerical models of piracy-triggered erosion waves and their role in pacing orogenic evolution. As mountain belts worldwide are experiencing accelerated climate change (Clark et al., 2024; Rae et al., 2021), understanding how past piracy events mediated feedbacks between erosion, rock uplift, and drainage stability becomes imperative for predicting landscape resilience to anthropogenic forcing.

6. Conclusions

In this study, the isochron burial dating method was utilized to ascertain the occurring age of a piracy event in northern Qilian Shan. Subsequently, χ analyses were conducted to explore the geomorphic feedbacks of the river piracy. From our research, the following conclusions can be drawn:

- (1) The Hongshuiba-Zhulongguan piracy occurred in the mid-Pleistocene, specifically around 0.79 ± 0.24 Ma;
- (2) The Zhulongguan River had been captured by the paleo-Beida River, which imprinted a legacy of χ profile flattening that persisted until the mid-Pleistocene piracy between the Hongshuiba River and Zhulongguan River;
- (3) The Hongshuiba-Zhulongguan piracy, maybe including the piracy in northern Qilian Shan, was driven by the regional tectonic-climatic coupling.

CRediT authorship contribution statement

Qi Su: Methodology, Investigation, Funding acquisition, Formal analysis, Data curation, Writing – review & editing, Writing – original draft. **Xianyan Wang:** Supervision, Formal analysis, Writing – review & editing, Writing – original draft. **Daoyang Yuan:** Supervision, Methodology, Investigation, Formal analysis, Writing – original draft. **Huiping Zhang:** Investigation, Funding acquisition, Conceptualization, Writing – review & editing. **Zhengchen Li:** Methodology, Investigation. **Hao Sun:** Investigation. **Hongqiang Li:** Methodology, Investigation.

Declaration of competing interest

The authors declare that they have no conflicts of interest in this work. We also declare that we do not have any commercial or associative interest that represents a conflict of interest in connection with the work submitted.

Acknowledgments

This research was supported by the National Natural Science Foundation of China (42225205, 42201004, 42488301). We thank Niannian Fan for assistance with χ analyses and Jingdong Zhao for laboratory

support. We are also grateful to William E. Odom and another anonymous reviewer for their insightful comments and constructive suggestions, which significantly improved the manuscript.

The authors declared that they have no conflicts of interest to this work.

Data availability

The authors confirm that all data necessary for supporting the scientific findings of this paper have been provided.

References

- Akçar, N., Ivy-Ochs, S., Alfimov, V., Schlunegger, F., Claude, A., Reber, R., Christl, M., Vockenhuber, C., Dehner, A., Rahn, M., 2017. Isochron-burial dating of glaciofluvial deposits: first results from the Swiss Alps. *Earth Surf. Process. Landf.* 42 (14), 2414–2425.
- Allen, M.B., Walters, R.J., Song, S., Saville, C., De Paola, N., Ford, J., Hu, Z., Sun, W., 2017. Partitioning of oblique convergence coupled to the fault locking behavior of fold-and-thrust belts: evidence from the Qilian Shan, northeastern Tibetan Plateau. *Tectonics* 36 (9), 1679–1698.
- Babault, J., Teixell, A., Struth, L., Van Den Driessche, J., Arboleya, M.L., Tesón, E., 2013. Shortening, structural relief and drainage evolution in inverted rifts: insights from the Atlas Mountains, the Eastern Cordillera of Colombia and the Pyrenees. *Geol. Soc. Lond. Spec. Publ.* 377 (1), 141–158.
- Balco, G., Rovey, C.W., 2008. An isochron method for cosmogenic-nuclide dating of buried soils and sediments. *Am. J. Sci.* 308 (10), 1083–1114.
- Bender, A.M., Amos, C.B., Bierman, P., Rood, D.H., Staisch, L., Kelsey, H., Sherrod, B., 2016. Differential uplift and incision of the Yakima River terraces, Central Washington State. *J. Geophys. Res. Solid Earth* 121 (1), 365–384.
- Bender, A.M., Lease, R.O., Corbett, L.B., Bierman, P.R., Caffee, M.W., Rittenour, T.M., 2020. Late Cenozoic climate change paces landscape adjustments to Yukon River capture. *Nat. Geosci.* 13 (8), 571–575.
- Berends, C.J., Köhler, P., Lourens, L.J., Wal, R.S.W., 2021. On the Cause of the Mid-Pleistocene transition. *Rev. Geophys.* 59 (2), e2020RG000727.
- Bian, S., Tan, X., Liu, Y., Fan, S., Gong, J., Zhou, C., Shi, F., Murphy, M.A., 2024. Orographic rainfall drives the Himalaya drainage divide to move north. *Geomorphology* 444, 108952.
- Bian, S., Tan, X., Zuza, A.V., Zhou, C., Shi, F., Liu, Y., Gong, J., 2025. How does the newly-formed drainage divide migrate after a river capture event? *Earth Planet. Sci. Lett.* 651, 119165.
- Bishop, P., 1995. Drainage rearrangement by river capture, beheading and diversion. *Prog. Phys. Geogr.* 19 (4), 449–473.
- Bonnet, S., 2009. Shrinking and splitting of drainage basins in orogenic landscapes from the migration of the main drainage divide. *Nat. Geosci.* 2 (11), 766–771.
- Borchers, B., Marrero, S., Balco, G., Caffee, M., Goehring, B., Lifton, N., Nishiizumi, K., Phillips, F., Schaefer, J., Stone, J., 2016. Geological calibration of spallation production rates in the CRONUS-Earth project. *Quat. Geochronol.* 31, 188–198.
- Bracciali, L., Najman, Y., Parrish, R.R., Akhter, S.H., Millar, I., 2015. The Brahmaputra tale of tectonics and erosion: early Miocene river capture in the Eastern Himalaya. *Earth Planet. Sci. Lett.* 415, 25–37.
- Cheng, F., Garzione, C.N., Mitra, G., Jolivet, M., Guo, Z., Lu, H., Li, X., Zhang, B., Zhang, C., Zhang, H., Wang, L., 2019. The interplay between climate and tectonics during the upward and outward growth of the Qilian Shan orogenic wedge, northern Tibetan Plateau. *Earth Sci. Rev.* 198, 102945.
- Chmeleff, J., von Blanckenburg, F., Kossett, K., Jakob, D., 2010. Determination of the ^{10}Be half-life by multicollector ICP-MS and liquid scintillation counting. *Nucl. Instrum. Methods Phys. Res., Sect. B* 268 (2), 192–199.
- Chu, Y., Zhu, L., Chen, W., Zhang, J., Yang, W., Tao, G., 2015. Geomorphology and Evolution of the Upper Shule River. *Quaternary Sciences* 35 (2), 465–474.
- Clark, P.U., Shakun, J.D., Rosenthal, Y., Köhler, P., Bartlein, P.J., 2024. Global and regional temperature change over the past 4.5 million years. *Science* 383 (6685), 884–890.
- Claude, A., Akçar, N., Ivy-Ochs, S., Schlunegger, F., Kubik, P.W., Christl, M., Vockenhuber, C., Kuhlemann, J., Rahn, M., Schlüchter, C., 2019. Changes in landscape evolution patterns in the northern Swiss Alpine Foreland during the mid-Pleistocene revolution. *GSA Bull.* 131 (11–12), 2056–2078.
- Corbett, L.B., Bierman, P.R., Rood, D.H., Caffee, M.W., Lifton, N.A., Woodruff, T.E., 2017. Cosmogenic $^{26}\text{Al}/^{10}\text{Be}$ surface production ratio in Greenland. *Geophys. Res. Lett.* 44 (3), 1350–1359.
- Dai, S., Fang, X., Song, C., Gao, J., Gao, D., Li, J., 2005. Early tectonic uplift of the northern Tibetan Plateau. *Chin. Sci. Bull.* 50 (15), 1642–1652.
- Ding, Z., Derbyshire, E., Yang, S., Yu, Z., Xiong, S., Liu, T., 2002. Stacked 2.6-Ma grain size record from the Chinese loess based on five sections and correlation with the deep-sea $\delta^{18}\text{O}$ record. *Paleoceanography* 17 (3), 1033.
- Erlanger, E.D., Granger, D.E., Gibbon, R.J., 2012. Rock uplift rates in South Africa from isochron burial dating of fluvial and marine terraces. *Geology* 40 (11), 1019–1022.
- Fan, N., Chu, Z., Jiang, L., Hassan, M.A., Lamb, M.P., Liu, X., 2018. Abrupt drainage basin reorganization following a Pleistocene river capture. *Nat. Commun.* 9 (1), 1–6.
- Fang, X., Garzione, C., Van der Voo, R., Li, J., Fan, M., 2003. Flexural subsidence by 29 Ma on the NE edge of Tibet from the magnetostratigraphy of Linxia Basin, China. *Earth Planet. Sci. Lett.* 210 (3–4), 545–560.

- Fox, M., 2019. A linear inverse method to reconstruct paleo-topography. *Geomorphology* 337, 151–164.
- Gallen, S.F., Wegmann, K.W., 2017. River profile response to normal fault growth and linkage: an example from the Hellenic forearc of south-Central Crete, Greece. *Earth Surface Dynamics* 5 (1), 161–186.
- Gnann, S., Baldwin, J.W., Cuthbert, M.O., Gleeson, T., Schwanghart, W., Wagener, T., 2025. The Influence of Topography on the Global Terrestrial Water Cycle. *Rev. Geophys.* 63 (1), e2023RG000810.
- Granger, D.E., Gibbon, R.J., Kuman, K., Clarke, R.J., Bruxelles, L., Caffee, M.W., 2015. New cosmogenic burial ages for Sterkfontein Member 2 Australopithecus and Member 5 Oldowan. *Nature* 522 (7554), 85–88.
- Granger, D.E., Stratford, D., Bruxelles, L., Gibbon, R.J., Clarke, R.J., Kuman, K., 2022. Cosmogenic nuclide dating of Australopithecus at Sterkfontein, South Africa. *Proc. Natl. Acad. Sci. USA* 119 (27), e2123516119.
- Han, W., Appel, E., Galy, A., Rösler, W., Fang, X., Zhu, X., Vandenberghe, J., Wang, J., Berger, A., Lü, S., Zhang, T., 2020. Climate transition in the Asia inland at 0.8–0.6 Ma related to astronomically forced ice sheet expansion. *Quat. Sci. Rev.* 248, 106580.
- Han, X., Dai, J.-G., Smith, A.G.G., Xu, S.-Y., Liu, B.-R., Wang, C.-S., Fox, M., 2024. Recent uplift of Chomolungma enhanced by river drainage piracy. *Nat. Geosci.* 17 (10), 1031–1037.
- He, P., Song, C., Wang, Y., Meng, Q., Wang, D., Feng, Y., Chen, L., Feng, W., 2020. Early Cenozoic exhumation in the Qilian Shan, northeastern margin of the Tibetan Plateau: Insights from detrital apatite fission track thermochronology. *Terra Nova* 32 (6), 415–424.
- He, C., Yang, C.-J., Turowski, J.M., Rao, G., Roda-Boluda, D.C., Yuan, X.-P., 2021. Constraining tectonic uplift and advection from the main drainage divide of a mountain belt. *Nat. Commun.* 12 (1), 544.
- He, C., Braun, J., Tang, H., Yuan, X., Acevedo-Trejos, E., Ott, R.F., Stucky de Quay, G., 2024. Drainage divide migration and implications for climate and biodiversity. *Nat. Rev. Earth & Environ.* 5 (3), 177–192.
- Herbert, T.D., 2023. The Mid-Pleistocene climate transition. *Annu. Rev. Earth Planet. Sci.* 51 (1), 389–418.
- Hetzell, R., Hampel, A., Gebbeken, P., Xu, Q., Gold, R.D., 2019. A constant slip rate for the western Qilian Shan frontal thrust during the last 200 ka consistent with GPS-derived and geological shortening rates. *Earth Planet. Sci. Lett.* 509, 100–113.
- Howard, A.D., Dietrich, W.E., Seidl, M.A., 1994. Modeling fluvial erosion on regional to continental scales. *J. Geophys. Res.* 99 (B7), 13971–13986.
- Hu, X., Pan, B., Kirby, E., Li, Q., Geng, H., Chen, J., 2010. Spatial differences in rock uplift rates inferred from channel steepness indices along the northern flank of the Qilian Mountain, northeast Tibetan Plateau. *Chin. Sci. Bull.* 55 (27–28), 3205–3214.
- Hu, G., Yi, C.-L., Zhang, J.-F., Liu, J.-H., Jiang, T., Qin, X., 2014. Optically stimulated luminescence dating of a moraine and a terrace in Laozugou valley, western Qilian Shan, northeastern Tibet. *Quat. Int.* 321, 37–49.
- Hu, K., Fang, X., Ferrier, K.L., Granger, D.E., Zhao, Z., Ruetenik, G.A., 2021. Covariation of cross-divide differences in denudation rate and χ : Implications for drainage basin reorganization in the Qilian Shan, Northeast Tibet. *Earth Planet. Sci. Lett.* 562, 116812.
- Jaiswara, N.K., Pandey, P., Pandey, A.K., 2019. Mio-Pliocene piracy, relict landscape and drainage reorganization in the Namcha Barwa syntaxis zone of eastern Himalaya. *Sci. Rep.* 9 (1), 17585.
- Jolivet, M., Brunel, M., Seward, D., Xu, Z., Yang, J., Roger, F., Tapponnier, P., Malavieille, J., Arnaud, N., Wu, C., 2001. Mesozoic and Cenozoic tectonics of the northern edge of the Tibetan plateau: fission-track constraints. *Tectonophysics* 343 (1–2), 111–134.
- Kirby, E., Whipple, K., 2001. Quantifying differential rock-uplift rates via stream profile analysis. *Geology* 29 (5), 415–418.
- Kirby, E., Whipple, K.X., 2012. Expression of active tectonics in erosional landscapes. *J. Struct. Geol.* 44, 54–75.
- Lai, J., Huppert, K., 2023. Asymmetric glaciation, divide migration, and postglacial fluvial response times in the Qilian Shan. *Geology* 51 (9), 860–864.
- Lai, J., Huppert, K., 2024. Climate-Driven Topographic Asymmetry Enhanced by Glaciers: Implications for Drainage Reorganization in Glacial Landscapes. *Geophys. Res. Lett.* 51 (13), e2024GL109087.
- Lavé, J., 2015. Landscape inversion by stream piracy. *Nature* 520 (7548), 442–444.
- Lease, R.O., Burbank, D.W., Clark, M.K., Farley, K.A., Zheng, D., Zhang, H., 2011. Middle Miocene reorganization of deformation along the northeastern Tibetan Plateau. *Geology* 39 (4), 359–362.
- Lisicki, L.E., Raymo, M.E., 2005. A Pliocene-Pleistocene stack of 57 globally distributed benthic 6180 records. *Paleoceanography and Paleoclimatology* 20 (2), PA1003.
- Litty, C., Schlunegger, F., Akçar, N., Delunel, R., Christl, M., Vockenhuber, C., 2018. Chronology of alluvial terrace sediment accumulation and incision in the Pativilca Valley, western Peruvian Andes. *Geomorphology* 315, 45–56.
- Liu, D., Fang, X., Song, C., Dai, S., Zhang, T., Zhang, W., Miao, Y., Liu, Y., Wang, J., 2010. Stratigraphic and paleomagnetic evidence of mid-Pleistocene rapid deformation and uplift of the NE Tibetan Plateau. *Tectonophysics* 486 (1–4), 108–119.
- Liu, W., Liu, Z., Sun, J., Song, C., Chang, H., Wang, H., Wang, Z., An, Z., 2020. Onset of permanent Taklimakan Desert linked to the mid-Pleistocene transition. *Geology* 48.
- Liu, Y., Wang, S., Xu, S., Fabel, D., Stuart, F.M., Rodés, Á., Zhang, X., Luo, W., 2022. New chronological constraints on the Plio-Pleistocene uplift of the Guizhou Plateau, SE margin of the Tibetan Plateau. *Quat. Geochronol.* 67, 101237.
- Luo, L., Granger, D.E., Tu, H., Lai, Z., Shen, G., Bae, C.J., Ji, X., Liu, J., 2020. The first radiometric age by isochron 26Al/10Be burial dating for the early Pleistocene Yuanmou hominin site, southern China. *Quat. Geochronol.* 55, 101022.
- Maher, E., Harvey, A.M., France, D., 2007. The impact of a major Quaternary river capture on the alluvial sediments of a beheaded river system, the Rio Alias SE Spain. *Geomorphology* 84 (3–4), 344–356.
- Mauffrey, M.-A., Urgeles, R., Berné, S., Canning, J., 2017. Development of submarine canyons after the Mid-Pleistocene transition on the Ebro margin, NW Mediterranean: the role of fluvial connections. *Quat. Sci. Rev.* 158, 77–93.
- Meng, K., Wang, E., Chu, J.J., Su, Z., Fan, C., 2020. Late Cenozoic river system reorganization and its origin within the Qilian Shan, NE Tibet. *J. Struct. Geol.* 138, 104128.
- Meyer, B., Tapponnier, P., Gaudemer, Y., Peltzer, G., Shunmin, G., Zhitai, C., 1996. Rate of left-lateral movement along the easternmost segment of the Altyn Tagh fault, east of 96° E (China). *Geophys. J. Int.* 124 (1), 29–44.
- Meyer, B., Tapponnier, P., Bourjot, L., Metivier, F., Gaudemer, Y., Peltzer, G., Shunmin, G., Zhitai, C., 1998. Crustal thickening in Gansu-Qinghai, lithospheric mantle subduction, and oblique, strike-slip controlled growth of the Tibet plateau. *Geophys. J. Int.* 135 (1), 1–47.
- Nishizumi, K., 2004. Preparation of 26Al AMS standards. *Nucl. Instrum. Methods Phys. Res., Sect. B* 223, 388–392.
- Odom, W.E., 2025. Pysochron: a Python-based solution for calculating cosmogenic 26Al/10Be isochron burial ages. *Quat. Geochronol.* 89, 101675.
- Odom, W.E., Granger, D.E., 2022. The Pliocene-to-present Course of the Tennessee River. *J. Geol.* 130 (4), 325–333.
- Pan, B., Chen, D., Hu, X., Cao, X., Chen, J., Mao, J., 2016. Drainage evolution of the Heihe River in western Hexi Corridor, China, derived from sedimentary and magnetostratigraphic results. *Quat. Sci. Rev.* 150, 250–263.
- Pang, J., Yu, J., Zheng, D., Wang, W., Ma, Y., Wang, Y., Li, C., Li, Y., Wang, Y., 2019. Neogene expansion of the Qilian Shan, North Tibet: Implications for the Dynamic Evolution of the Tibetan Plateau. *Tectonics* 38 (3), 1018–1032.
- Penserini, B.D., Morell, K.D., Codilean, A.T., Fülöp, R.H., Wilcken, K.M., Yanites, B.J., Kumar, A., Fan, S., Mearee, T., 2024. Magnitude and timing of transient incision resulting from large-scale drainage capture, Sutlej River, Northwest Himalaya. *Earth Surf. Process. Landf.* 49 (1), 334–353.
- Perron, J.T., Royden, L., 2013. An integral approach to bedrock river profile analysis. *Earth Surf. Process. Landf.* 38 (6), 570–576.
- Rae, J.W.B., Zhang, Y.G., Liu, X., Foster, G.L., Stoll, H.M., Whiteford, R.D.M., 2021. Atmospheric CO₂ over the past 66 Million Years from Marine Archives. *Annu. Rev. Earth Planet. Sci.* 49 (1), 609–641.
- Rong, J., Wang, Y., Zhan, R., Fan, J., Huang, B., Tang, P., Li, Y., Zhang, X., Wu, R., Wang, G., Wei, X., 2019. Silurian integrative stratigraphy and timescale of China. *Sci. China Earth Sci.* 62 (1), 89–111.
- Sánchez Goñi, M.F., Ferretti, P., Polanco-Martínez, J.M., Rodrigues, T., Alonso-García, M., Rodríguez-Tovar, F.J., Dorador, J., Desprat, S., 2019. Pronounced northward shift of the westerlies during MIS 17 leading to the strong 100-kyr ice age cycles. *Earth Planet. Sci. Lett.* 511, 117–129.
- Schwanghart, W., Scherler, D., 2014. Short Communication: TopoToolbox 2 – MATLAB-based software for topographic analysis and modeling in Earth surface sciences. *Earth Surf. Dyn.* 2 (1), 1–7.
- Schwanghart, W., Scherler, D., 2020. Divide mobility controls knickpoint migration on the Roan Plateau (Colorado, USA). *Geology* 48 (7), 698–702.
- Seong, Y.B., Kang, H.-C., Ree, J.-H., Choi, J.-H., Lai, Z., Long, H., Yoon, H.O., 2011. Geomorphic constraints on active mountain growth by the lateral propagation of fault-related folding: a case study on Yumu Shan, NE Tibet. *J. Asian Earth Sci.* 41 (2), 184–194.
- Shugar, D.H., Clague, J.J., Best, J.L., Schoof, C., Willis, M.J., Copland, L., Roe, G.H., 2017. River piracy and drainage basin reorganization led by climate-driven glacier retreat. *Nat. Geosci.* 10 (5), 370–375.
- Struth, L., Teixell, A., Owen, L.A., Babault, J., 2017. Plateau reduction by drainage divide migration in the Eastern Cordillera of Colombia defined by morphometry and 10Be terrestrial cosmogenic nuclides. *Earth Surf. Process. Landf.* 42 (8), 1155–1170.
- Struth, L., Giachetta, E., Willett, S.D., Owen, L.A., Tesón, E., 2020. Quaternary drainage network reorganization in the Colombian Eastern Cordillera Plateau. *Earth Surf. Process. Landf.* 45 (8), 1789–1804.
- Su, Q., Wang, X., Lu, H., Zhang, H., Xie, H., 2022. River piracy and its geomorphic effects in the northern Qilian Shan, northeastern Qinghai-Tibet Plateau. *Palaeogeogr. Palaeoclimatol. Palaeoecol.* 601, 111147.
- Su, Q., Wang, X., Yuan, D., Xie, H., Li, H., Huang, X., 2023. Fluvial entrenchment of the Gonghe Basin and integration of the upper Yellow River - evidence from the cosmogenically dated geomorphic surfaces. *Geomorphology* 429, 108654.
- Tu, H., Shen, G., Granger, D., Yang, X., Lai, Z., 2017. Isochron 26Al/10Be burial dating of the Lantian hominin site at Gongwangling in Northwestern China. *Quat. Geochronol.* 41, 174–179.
- Tu, H., Luo, L., Deng, C., Ou, Z., Lai, Z., Shen, G., Bae, C.J., Granger, D., 2022. Isochron 26Al/10Be burial dating of the Xiashagou Fauna in the Nihewan Basin, northern China: Implications for biogeography and early hominin dispersals. *Quat. Sci. Rev.* 283, 107447.
- Wang, Y., Zhang, H., Zheng, D., Zheng, W., Zhang, Z., Wang, W., Yu, J., 2014. Controls on decadal erosion rates in Qilian Shan: Re-evaluation and new insights into landscape evolution in north-East Tibet. *Geomorphology* 223, 117–128.
- Wang, Y., Zheng, D., Zhang, H., Li, C., Xiao, L., Li, Y., Hao, Y., 2019. The distribution of active rock uplift in the interior of the western Qilian Shan, NE Tibetan Plateau: Inference from bedrock channel profiles. *Tectonophysics* 759, 15–29.
- Wang, Y., Goren, L., Zheng, D., Zhang, H., 2022a. Short communication: Forward and inverse analytic models relating river long profile to tectonic uplift history, assuming a nonlinear slope-erosion dependency. *Earth Surf. Dyn.* 10 (4), 833–849.

- Wang, Y., Zheng, D., Zhang, H., 2022b. The methods and program implementation for river longitudinal profile analysis—RiverProAnalysis, a set of open-source functions based on the Matlab platform. *Sci. China Earth Sci.* 65 (9), 1788–1809.
- Waters, J.M., Wallis, G.P., Burridge, C.P., Craw, D., 2015. Geology shapes biogeography: Quaternary river-capture explains New Zealand's biologically 'composite' Taieri River. *Quat. Sci. Rev.* 120, 47–56.
- Whipple, K.X., 2004. Bedrock rivers and the geomorphology of active orogens. *Annu. Rev. Earth Planet. Sci.* 32, 151–185.
- Whipple, K.X., DiBiase, R.A., Ouimet, W.B., Forte, A.M., 2017a. Preservation or piracy? Diagnosing low-relief, high-elevation surface formation mechanisms. *Geology* 45 (1), 91–94.
- Whipple, K.X., Forte, A.M., Dibiase, R.A., Gasparini, N.M., Ouimet, W.B., 2017b. Timescales of landscape response to divide migration and drainage capture: Implications for the role of divide mobility in landscape evolution. *J. Geophys. Res. Earth* 122, 248–273.
- Willett, S.D., 2025. How do mountains grow? *Nat. Rev. Earth & Environ.* 6 (1), 6.
- Willett, S.D., Mccoy, S.W., Perron, J.T., Goren, L., Chen, C.Y., 2014. Dynamic reorganization of river basins. *Science* 343 (6175), 1248765.
- Wobus, C., Whipple, K.X., Kirby, E., Snyder, N., Johnson, J., Spyropoulos, K., Crosby, B., Sheehan, D., Willett, S.D., Hovius, N., Brandon, M.T., Fisher, D.M., 2006. Tectonics from topography: Procedures, promise, and pitfalls. *Tectonics, climate, and Landscape Evolution. Geolo. Soc. Am.* 55–74.
- Yang, R., Willett, S.D., Goren, L., 2015a. In situ low-relief landscape formation as a result of river network disruption. *Nature* 520 (7548), 526–529.
- Yang, X., Scuderi, L.A., Wang, X., Scuderi, L.J., Zhang, D., Li, H., Forman, S., Xu, Q., Wang, R., Huang, W., Yang, S., 2015b. Groundwater sapping as the cause of irreversible desertification of Hunshandake Sandy Lands, Inner Mongolia, northern China. *Proc. Natl. Acad. Sci. USA* 112 (3), 702–706.
- Yang, H., Yang, X., Huang, X., Li, A., Huang, W., Zhang, L., 2018. New constraints on slip rates of the Fodongmiao-Hongyazi fault in the Northern Qilian Shan, NE Tibet, from the 10 be exposure dating of offset terraces. *J. Asian Earth Sci.* 151, 131–147.
- Yang, R., Suhail, H.A., Gourbet, L., Willett, S.D., Fellin, M.G., Lin, X., Gong, J., Wei, X., Maden, C., Jiao, R., Chen, H., 2020. Early Pleistocene drainage pattern changes in Eastern Tibet: Constraints from provenance analysis, thermochronometry, and numerical modeling. *Earth Planet. Sci. Lett.* 531, 115955.
- Ye, Y., Tan, X., Liu, Y., Bian, S., Zhou, C., Zeng, X., Shi, F., Gao, M., 2024. Drainage reorganization and divide migration driven by basin subsidence: An example from the Micang Shan, outskirts of eastern Tibet and its implications for Cenozoic evolution of the Yangtze River. *Basin Res.* 36 (3), e12875.
- Yin, Z., Xu, S., 1992. Research on Qilian Mountain Landform and Cartography. Science Press, Beijing.
- Yin, A., Dang, Y.-Q., Wang, L.-C., Jiang, W.-M., Zhou, S.-P., Chen, X.-H., Gehrels, G.E., McRivette, M.W., 2008. Cenozoic tectonic evolution of Qaidam basin and its surrounding regions (part 1): the southern Qilian Shan-Nan Shan thrust belt and northern Qaidam basin. *Geol. Soc. Am. Bull.* 120 (7–8), 813–846.
- Yu, J., Pang, J., Wang, Y., Zheng, D., Liu, C., Wang, W., Li, Y., Li, C., Xiao, L., 2019. Mid-Miocene uplift of the northern Qilian Shan as a result of the northward growth of the northern Tibetan Plateau. *Geosphere* 15 (2), 423–432.
- Yuan, D.-Y., Ge, W.-P., Chen, Z.-W., Li, C.-Y., Wang, Z.-C., Zhang, H.-P., Zhang, P.-Z., Zheng, D.-W., Zheng, W.-J., Craddock, W.H., Dayem, K.E., Duvall, A.R., Hough, B.G., Lease, R.O., Champagnac, J.-D., Burbank, D.W., Clark, M.K., Farley, K.A., Garzione, C.N., Kirby, E., Molnar, P., Roe, G.H., 2013. The growth of northeastern Tibet and its relevance to large-scale continental geodynamics: a review of recent studies. *Tectonics* 32 (5), 1358–1370.
- Zachos, J., Pagani, M., Sloan, L., Thomas, E., Billups, K., 2001. Trends, Rhythms, and Aberrations in Global climate 65 Ma to present. *Science* 292 (5517), 686–693.
- Zhang, Y., Zhan, R., Zhen, Y., Wang, Z., Yuan, W., Fang, X., Ma, X., Zhang, J., 2019. Ordovician integrative stratigraphy and timescale of China. *Sci. China Earth Sci.* 62 (1), 61–88.
- Zhang, Y., Zhang, H., Ma, Z., Wang, Y., Zhao, X., 2023. Inversion of late Miocene uplift history from the transient Daxia River landscape, NE Tibetan Plateau. *J. Geol. Soc. Lond.* 180 (6).
- Zhao, Z., Granger, D., Zhang, M., Kong, X., Yang, S., Chen, Y., Hu, E., 2016. A test of the isochron burial dating method on fluvial gravels within the Pulu volcanic sequence, West Kunlun Mountains, China. *Quat. Geochronol.* 34, 75–80.
- Zhao, J., Qiu, J., Harbor, J.M., Ji, H., Caffee, M.W., Guo, W., Zheng, H., 2023. Timing and extent of late Quaternary glaciations on Karlik Mountain, eastern Tianshan range, China. *Quat. Sci. Rev.* 306, 108038.
- Zheng, D., Clark, M.K., Zhang, P., Zheng, W., Farley, K.A., 2010. Erosion, fault initiation and topographic growth of the North Qilian Shan (northern Tibetan Plateau). *Geosphere* 6 (6), 937–941.
- Zheng, W.J., Zhang, P.Z., Ge, W.P., Molnar, P., Zhang, H.P., Yuan, D.Y., Liu, J.H., 2013. Late Quaternary slip rate of the South Heli Shan Fault (northern Hexi Corridor, NW China) and its implications for northeastward growth of the Tibetan Plateau. *Tectonics* 32 (2), 271–293.
- Zheng, D., Wang, W., Wan, J., Yuan, D., Liu, C., Zheng, W., Zhang, H., Pang, J., Zhang, P., 2017. Progressive northward growth of the northern Qilian Shan-Hexi Corridor (northeastern Tibet) during the Cenozoic. *Lithosphere* 9 (3), 408–416.
- Zheng, Y., Li, H., Pan, J., Gong, Z., Wang, P., Lai, Y., Zhao, Z., Liu, F., 2023. Mid-Pleistocene drainage rearrangement of the Dadu River in response to plate convergence in southeastern Tibet. *Quat. Res.* 114, 130–147.
- Zhou, J., Zhou, W., Dong, G., Hou, Y., Xian, F., Zhang, L., Tang, L., Zhao, G., Fu, Y., 2020. Cosmogenic 10Be and 26Al exposure dating of Nam Co lake terraces since MIS 5, southern Tibetan Plateau. *Quat. Sci. Rev.* 231.
- Zuza, A.V., Wu, C., Reith, R.C., Yin, A., Li, J., Zhang, J., Zhang, Y., Wu, L., Liu, W., 2017. Tectonic evolution of the Qilian Shan: An early Paleozoic orogen reactivated in the Cenozoic. *GSA Bull.* 130 (5/6), 881–925.
- Zuza, A.V., Wu, C., Wang, Z., Levy, D.A., Li, B., Xiong, X., Chen, X., 2018. Underthrusting and duplexing beneath the northern Tibetan Plateau and the evolution of the Himalayan-Tibetan orogen. *Lithosphere* 11 (2), 209–231.